© Universiti Tun Hussein Onn Malaysia Publisher's Office

IJIE

Journal homepage: http://penerbit.uthm.edu.my/ojs/index.php/ijie
ISSN : 2229-838X e-ISSN : 2600-7916

The International Journal of Integrated Engineering

Effect of FSW Parameters on the Microstructure and Mechanical Properties of T-joints between Dissimilar Al-Alloys

Mohamed M. El-Sayed Seleman[1,2], Mohamed M. Z. Ahmed[1,2,3], Rashad M. Ramadan[1], Basant A. Zaki[1*]

[1]Metallurgical and Materials Engineering Department,
Faculty of Petroleum and Mining Engineering. Suez University, Al-salam 1, Suez, 43721, EGYPT

[2]Suez and Sinai Metallurgical and Materials Research Center of Scientific Excellence (SSMMR-CSE),
Suez University, Al-salam 1, Suez, 43721, EGYPT

[3]Mechanical Engineering Department, College of Engineering at Al Kharj,
Prince Sattam Bin Abdulaziz University, Al Kharj 11942, KSA

*Corresponding author

DOI: https://doi.org/10.30880/ijie.2022.14.01.001
Received 7 August 2021; Accepted 5 February 2021; Available online 07 March 2022

Abstract: The main purpose of this research is to develop T-joints between the aluminum AA 2024-T4 and AA 7075-T6 using friction stir welding. The effect of tool geometries, tool traveling speed, and rotational rate in the welded T-joints were investigated and discussed. Three different tools were used with different shoulder to pin ratios 3.28, 3.36, and 4.31. After optimization, the best tool dimension has used with the different rotational and welding speeds. Three tool traverse speeds of 50, 75, and 100 mm/min were used. Two rotation rates of 800 rpm and 1000 rpm were applied. After FSW, at a number of the above FSW parameters' combinations, macrostructure and microstructure analyses were done using optical microscopy. In order to have an insight into the mechanical properties, hardness measurements and tensile testing were carried out. Using small shoulder to pin ratio produced visually unacceptable T-joint. Opposite happened by using the tool with 4.31 of shoulder to pin ratio. Furthermore, the results showed sound T-welds with no obvious defects at high rotational rate of 1000 rpm with the two used traveling speeds. Asymmetric temperature distribution was observed between the two sides, advance side (AS) and retreating side (RS

Keywords: Friction stir welding; AA2024; AA7075; T-joints; dissimilar weld

1. Introduction

Heat treatable aluminium alloys are difficult to weld by traditional welding techniques. Therefore, Friction Stir Welding (FSW) process is used where melting temperature is sidestepped. A novel solid-state welding process, Friction Stir Welding (FSW), is invented in 1991 by The Welding Institute (TWI) of UK. Joining aluminum alloys by traditional fusion welding methods lead to considerable decrease in the mechanical properties and due to the necessity of aluminum alloys in aeronautical application, a strong tendency for joining these alloys without mechanical deterioration was a demand. Therefore, FSW technique was firstly applied for aluminum alloys[1-3]. FSW allowing quality improvements on the product. Also, it generates a wide range of advantages over the traditional fusion welding

*Corresponding author: basant.zaki@suezuni.edu.eg

techniques. The reason behind the advantages of FSW over the other traditional welding methods is because it is a solid-state joining process where the joining process takes place without reaching the melting temperature of the alloy [3]. By avoiding melting, defects that related to solidification will be eliminated or considerably reduced such as porosity, segregation, hot crack, and dendritic structure formation. The heat input in FSW joint is less than other joining process, in this way, fewer residual stresses are predicted. FSW is a clean process with respect to other process where shielding gases are not necessary, and fumes are not produced [4]. A rotating tool with a shoulder and pin generates heat in FSW by the friction between the tool and the workpieces allowing material softening [5]. The soft material transfers from the advancing side (AS) to the retreating side (RS) of the joint, also up down transformation, leading to a bond between the plates. Heat generated and material flow depend on different parameters in FSW process which directly affect the quality of T-joints [6].

To obtain free-defect T-joints, the welding parameters have to set up experimentally for each tool shape. In particular, the best relation between the rotational rate of the tool and its traveling speed, it is important to define, which affected not only heat generation but also the quality of mixing and dwell time of the material at elevated temperature [7, 8]. Thus, many of the welding parameters (welding speed/rotational tool speed) were examined to determined one set of parameters for which FSW T-joints exhibited the highest welding quality. Friction stir welded joints, have three main different regions. Each region has its own micro- features and mechanical features [9]. Starting from the middle of the weld line, the stir zone (SZ), a fine equiaxed grain is formed as a result of recrystallization mechanisms that the combination of heat, forging and stirring leads to. Next, around the (SZ), the thermo-mechanical affected zone (TMAZ) region shows a high dislocation density as well as coarsening of the strengthening precipitates of the aluminum alloy. Finally, the heat affected zone (HAZ) where hardening precipitates have been dissolved or seemed coarser as compared to the base material [10].

The uses of 2024 and 7075 aluminum alloys (AA) in automotive sector and aerospace industry due to their high strength to weight ratio increases the demand for joining these alloys by FSW welding instead of fastener, riveting, or fusion welding techniques to achieve quality and performance improvements [11]. Because the high demand of 2024 and 7075AA, they were also friction stir processed to achieve better surface and mechanical properties for industrial uses [12, 13]. These two alloys are often used in a complex profile where the AA2024 is a large sheet used for the body structures, called skin and a specific stiffeners AA7075 used as a stringer of a T-joint combinations. Different shapes of T-joint combination are usually used, such as ‘‘Z’’ and ‘‘L’’[14, 15]. Despite the quite large number of researches on FSW during the last few years, it is worth to note that they are mostly focused on butt joints and the knowledge developed cannot directly be transferred to the T-joints, for which several characteristic, must be considered [4, 16, 17]. In aerospace industry, cladded plates of aluminum alloys are necessary for corrosion and protection reasons. These plates are a sandwich like shape of high-strength aluminum alloy between two sheets of commercially pure metal for maximizing the strength and improving the corrosion resistance. Therefore, joining cladded AA2024 and 7075 with the existence of a cladded layer has a great benefit in this sector. Acerra et al. [18], noticed the negative impact of the cladded layer in joining at specific welding conditions. In their study, in some cases, they removed the cladding layer for better joining. Thus, the aim of the current study is to conduct the FSW of the two aluminum alloys in T-joint configuration at different welding conditions with the existence of the cladding layer and study its effect on the quality and properties of the joint.

2. Experimental Procedure

The materials used in this research are 4 *mm* thick AA2024-T4 (cladded sheet), and 5 *mm* thick AA7075-T6, the former used as a skin and the latter used as a stringer. The aluminum plates were shaped in rectangular dimensions with 200 *mm* length and 100 *mm* width. Using a specially designed fixture as shown in Figure 1, the two plates are hold in a T-shape configuration in the friction stir welding machine (EG-FSW-M1), locally designed and manufactured in Egypt. The designed rotational tools were machined to end with a tapered cylindrical shape pin from tool steel (H13) and heat treated to obtain a hardness value of 58 HRC for conducting the FSW trials to produce the dissimilar Al alloys T-joints. All the tools have the same shape but with different dimensions. The main dimensions of the three tools are mentioned in **Error! Reference source not found.**. the shape of the third tool is shown in Fig. **2**.

The process conditions were chosen based on the previous studies [18, 19].The welding process was performed in two different rotational rates 800 and 1000 *rpm* and three different travel speeds 50, 75 and 100 *mm/min* as shown in

. All the other conditions were kept constant, such as tool tilt angle was 3 degree and plunge rate kept 1 *mm/sec*. For microstructure and mechanical investigation of the FSWed T-joint, three welded specimens were sectioned perpendicularly to the welding direction as shown in Fig. **3**. Dotted lines in this figure indicating the cutting lines for the three specimens. One specimen is used for micro and macro structure investigation and Vickers hardness test while the others two used for the tensile test. For hardness and microstructure investigation the dimension was 100 *mm X* 15 *mm X* 35 *mm* while the tensile test specimens' dimensions were 100 *mm X* 25 *mm X* 35 *mm*. For microstructure characterization, the specimens were prepared by grinding, polishing using the standard metallographic technique. After that, the specimens' surface was etched using Keller's reagent to reveal grain boundaries and other microstructures features.

Fig. 1 - A photograph for the adaptive fixture to weld 2024and 7075Al alloys in a T-joint configuration.

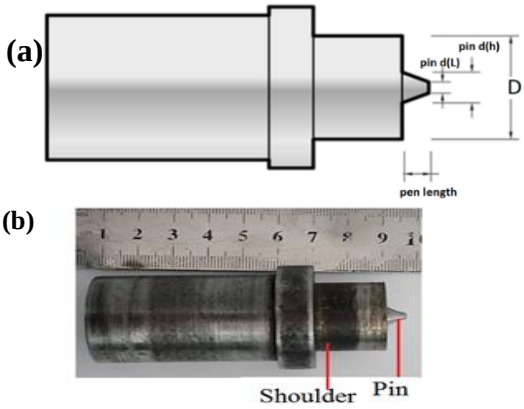

Fig. 2 - (a) a schematic illustration of the tool dimensions, (b) A photograph of the machined tool used in FSW experiments

Table 1 - Dimensions of the used tools

Tool	1st	2nd	3rd
Shoulder diameter (D)mm	16.8	17.4	25
Pin Diameter (h) mm	6	6.4	7.4
Pin Diameter (L) mm	3	2.9	2.7
Pin diameter at the upper 1/3 of the pin (d)	5	5.3	5.8
D/d	3.36	3.28	4.31
Pin length mm	5	5.8	6

Table 2 - Sample ID

Sample ID	Tool rotation speed (rpm)	Tool transverse speed (mm/min)
H-50	1000	50
L-50	800	50
L-100	800	100
H-100	1000	100
L-75	800	75

Fig. 3 - (a) the welded specimen of the T- joint before cutting; (b) A part specimen of T-joint after cutting perpendicular to the welding direction

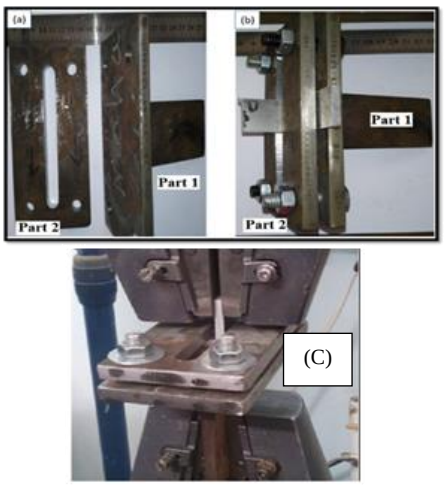

Fig. 4 - (a) and (b) photographs of clamping device for the tensile test without and with specimen, respectively; (c) a photograph of the clamping device attached to the tensile machine

Tensile test was done using model (Instron-M4208), at load 300 kN at room temperature with a cross-head speed 1mm/min for evaluation the weld mechanical properties along the skin (X- axis) and along the stranger (Y-axis) using a special clamping fixture as shown in Fig. **4**. After tensile fracture locations of samples were observed and photographed. Hardness measurements were measured using Vickers hardness tester (HWDV-75, TTS Unlimited, Osaka, Japan) to evaluate the hardness profiles with 2 kgf load and 15s dwelling time at regular intervals of 0.5 mm between each point as shown in Fig. **5**. 0.5 mm represents more than 2.5 times the maximum indentation diameter.

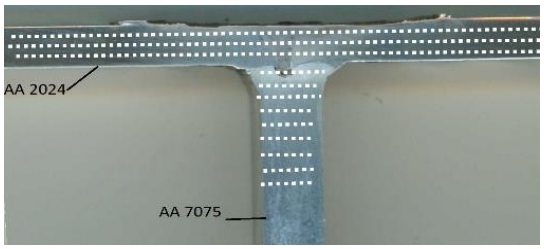

Fig. 5 - Hardness measuring points along the traversal cross section in the FSW T-joint specimen

3. Results and Discussion

3.1 Metallurgical Characterization

From **Error! Reference source not found.**, using the described 1st and 2nd tools produced a T-joint with a surface grove along the welding line which may be attributed to low heat input and insufficient material flow to fill the grove, as shown in Fig. **6** . This defect makes the joints unacceptable visually when using these tool dimensions. On the other hand, all the resulted T-joints welded by the 3rd tool were free from any visual defects and they welded successively using the described welding parameters in the experimental section,

. Three tool traverse speeds of 50, 75, and 100 *mm/min* were used with two rotation rates of 800 *rpm* and 1000 *rpm*. Therefore, this tool is the one used throughout the research. From that, it could be concluded that changing the shoulder and pin dimensions play a vital role in the amount of the generated heat which directly affect the material plasticity and its flow. We could conclude that tool geometry or dimension is responsible for determining the weld quality with maintaining the other welding parameters constant, this conclusion is in accordance with other reported by Raouache et. al.[20].

Therefore, between the suggested and designed three tools, the third tool with higher shoulder dimeter and higher D/d ratio, worked the best with the given friction stir welding parameter and used Aluminum alloys. Material hot deformed by the friction stir tool must be able to fill the void produced by a traversing pin. If the tool design is incorrect (i.e., pin diameter was too large for the selected parameters) or the travel speed was too fast, the hot deformed material will cool before the material can fully fill the region directly behind the tool. In addition, the shoulder is needed to keep enough heat to allow material flow around the tool; if insufficient heat is generated (through insufficient forging pressure or incorrect shoulder diameter), then material will not flow properly, and holes or groves will be form.

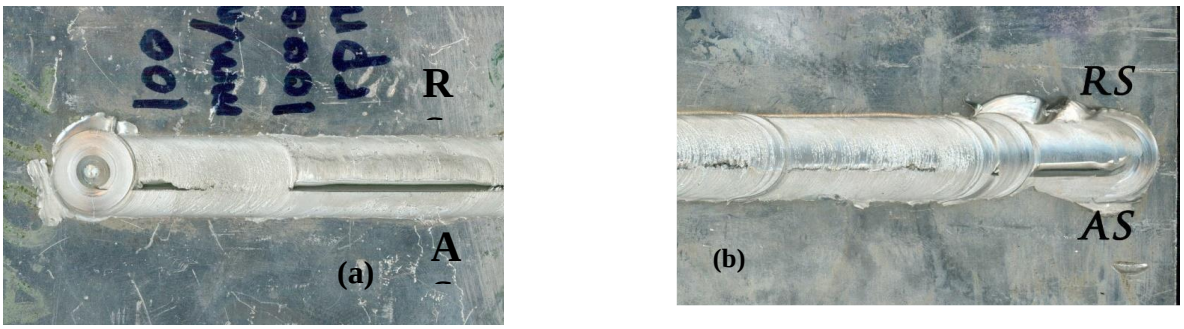

Fig. 6 - Two welded T-joint at the same welding conditions rotational rate 1000 rpm with traverse speed 100 mm/min but with two different tools. (a) using the 1st tool (D/d) =3.36; (b) using the 2nd tool (D/d) =3.28

Flash was observed in all the cases, but it was much more in some cases such as 800 *rpm* with 75 *mm/min* and 1000 *rpm* with 100 *mm/min*. The flash formation may be attributed to either deep plunge depth or high applied force by the tool or due to excessive heat input; e.g. high rotational rate and/or low traversal speed [21]. From macrostructure investigation, two welded T-joints produced a large tunnel defect in the advance side of the weld joint at 800 rpm with 50 and 75 *mm/min* traversal speed using the third tool, as shown in Fig. 7: (a) and (b), respectively. At the same rotational rate (800 *rpm*), but unpredictably higher traversal speed (100 *mm/min*), smaller defect was observed Fig. 7:

(c). This may be due to the position of the section taken which not represent the actual size of the tunnel along the weld length. On the other hand, Fig. 7: (d) and (e), no tunnel defect was observed at 1000 *rpm* with 50 and 100 *mm/min* traversal speed, respectively. In Fig. 7: (d) and (e) welded at 1000 *rpm* with 50 *mm* and 100 *mm*, respectively, better mixing between the two used alloys and the cladding layer were observed. This result could be attributed to the rate of material flow in the former where the traversal speed is high, and to high rotational rate of (1000 *rpm*) that in turn increases the generated heat in the two latter conditions

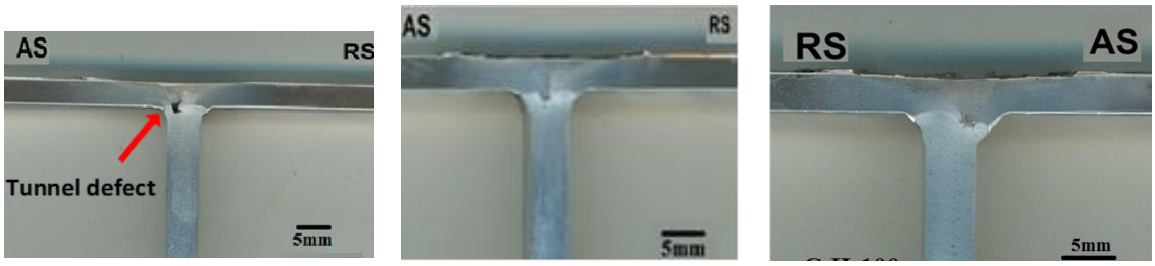

Fig. 7 - Macrostructures of joints welded at different welding conditions and using only the third tool

It can be considered that during the welding process of T- joints, cavities form preliminary in AS, and immediately, flowing materials in other regions fill these cavities to form a sound weld. If the fulfillment is insufficient or lagging, these cavities will remain inside the weld. As a result, a tunnel defect forms when the welding process has finished formation of tunnel defect at 800 rpm may be caused because of the insufficient material flow and low heat input, so the material plasticity is not enough to fill the formed cavities at the advance side [22]. Obviously, the tunnel defects in the T-joints is mainly produced by lacking material on the AS, which is accredited to a temperature distribution across the skin material. There is a vertical decrease in temperature and consequently increase in flow stress from top to bottom of the nugget zone. Therefore, the material ability to flow is easier near the top whereas the flow near the bottom remains heavily sluggish and need much forging force. So, the material which is required to refill the cavity left behind by the advancing tool is lacking resulting in tunnel. The flow stress harshly increases from top to bottom and material transport on the AS is considerably greater in comparison to that on RS. By increasing the weld speed from 50 to 100 *mm/min* the cooling rate increases and consequently this enhances the drop-in temperature from top to bottom. As a result, the flow stress severally increases which results a greater size of the tunnel.

We should put on consideration the existence of the cladding layer (commercial pure aluminum alloys with zinc) which act as a third material in this joint beside AA2024 and AA7075 because it has different physical and mechanical properties which is quite different than the two other alloys. If we accepted the welding temperature at the operated parameters around 450^{o}C [23], then the homologous temperatures for thermomechanical deformed in the stirred zone 7075, 2024 and commercial Al are almost 0.95, 0.92 and 0.79 respectively. Therefore, the ability to flow and mix with each other is different which makes the expectation to many different defects is high. Acerra et. al. [18]. detected a corner tunnel defect and a sort of hooking effect is observed with macro- voids at the end of the coating layer inside the T-joint transverse section for the AA2024-AA7075 T-joints. The resulted microstructure after FSW consisted of three new zones and the base alloys. These zones, starting from the place of the pin, are the stir zone (SZ), the thermo-mechanical affected zone (TMAZ) and the heat affected zone (HAZ), as shown in Fig. 8.

Table 1 - Grain size of the stir zone for each condition

FSW Condition	L-50	L-100	H-50	H-100
Grain size of the stir zone (μm)	4.6±0.8	4.7±0.7	6.46±1	5.1±0.6

From micro- and macro- structure analysis some features were noticed. Firstly, the grains in the stir zone for both materials are undergoing a dynamic recrystallization to form a new fine and equiaxed grains with average size 2.3±0.4 and 5.5 ±1.5 μm in diameter for 7075 and 2024 aluminum alloys, respectively as listed in Table 1 , and shown in Fig. 9. From that, we could conclude that the started grain size affects the resulted microstructure in dynamic recrystallization during FSW, which in turn improve the mechanical properties of this region [24]. Therefore, different materials have different responses to the FSW process even if the used FSW parameters were the same. This result was consistent with what has been found in a previous study by Ahmed et. al.[19] who found that the recrystallization process was different at the same FSW conditions for AA7075 than in AA5083.

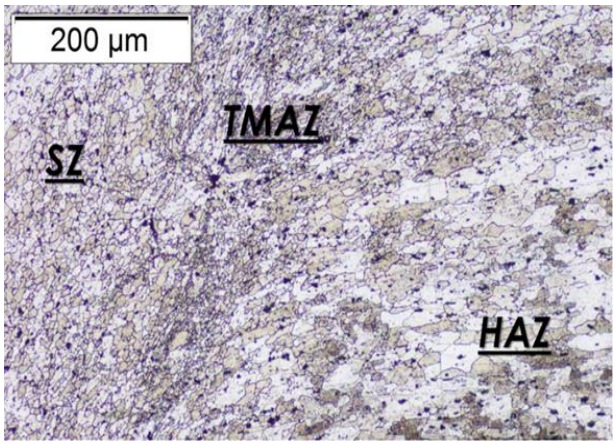

Fig. 8 - Optical microstructure of the FSWed T-joint AA2024-AA7075 at the interface between the NG zone and the TMAZ with some part of the HAZ

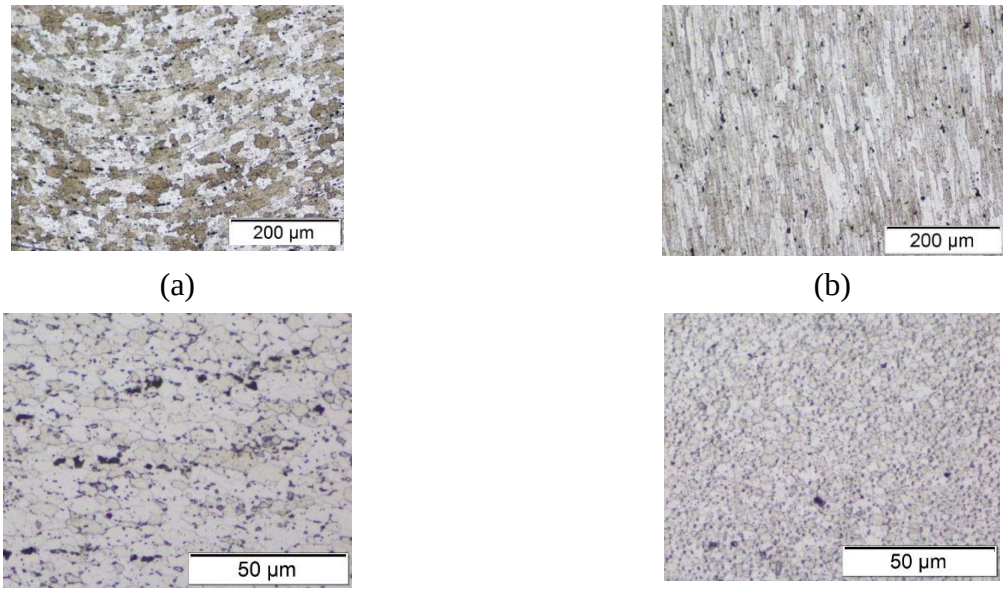

Fig. 9 - Optical microstructures base metal (BM) (a)2024-T4, (b) 7075-T6; (c) SZ of AA2024; (d) AA7075 both for C-L-100

The large grain size in the SZ at higher rotational rate is attributable to higher heat input. Same result was observed as in Fig. **8**: (b) and (d) at traverse speed 100 *mm/min* for 800 and 1000 *rpm*, respectively. More features were observed, for example, the transition zone between the TMAZ and the SZ was sharper and smaller in advance side than on the retreating side, as shown in Fig. 9. This result confirmed with that obtained in other work [15]. Results indicate that there is an obvious asymmetric temperature distribution between the advancing side (AS) and the retreating side (RS). This result was also noticed in the work of Jingming et. al. [27] by investigating a numerical simulation and experimental investigation for lap joint of the same alloys welded by FSW. Moreover, the unsymmetrical properties of the AS and the RS was noticed also in the hardness value in previous studies, Dudzik [28]. More about the asymmetric characterization between the advancing and retreating weld in FSW was observed in Raja et.al.[29]. In Fig. 10, the thickness of the cladding layer in the RS was 200 μm and it reached to 100 μm in the AS. Also, the grain under the cladding layer in the AS was refined and equiaxed while in the RS the grains were kept as it was, as received (7075-T6) which indicate a non-mixing condition. The existence and thickness of cladding layer indicate the quality of mixing between the two alloys during FSW Also, it implies the asymmetric temperature distribution between the two sides, AS and RS. For that, we could conclude that the AS undergoes higher temperature and stirring when compare with the RS for the same FSW condition.

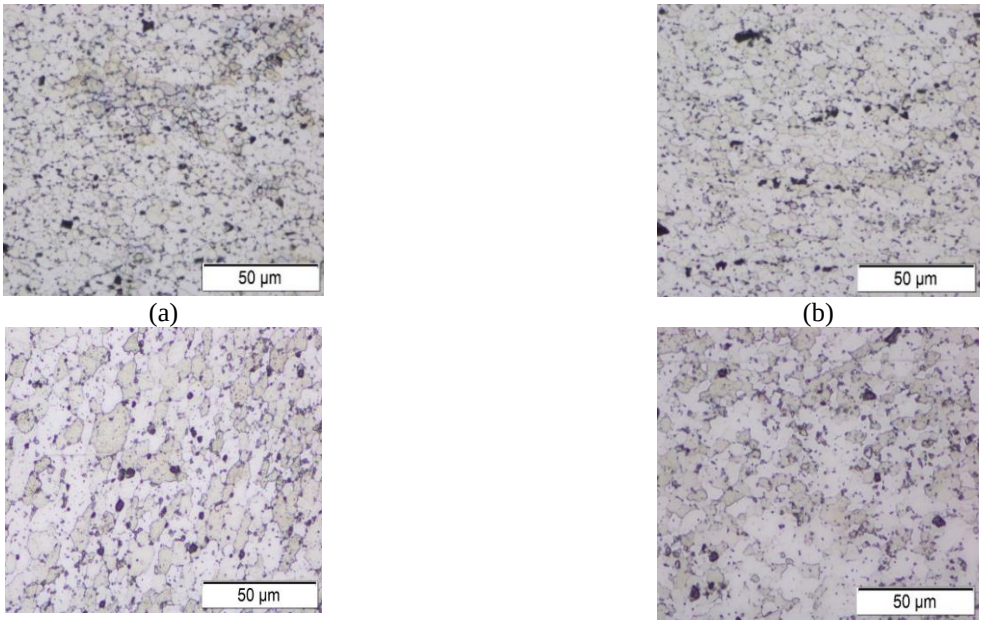

Fig. 8 - Optical microstructures of the SZ of the joints at (a) L-50; (b) L-100; (c) H-50 (d) H-100

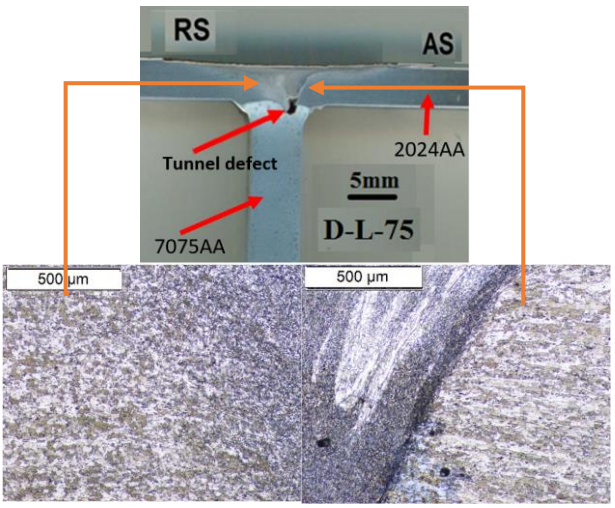

The transition zone in the RS

The transition zone in the AS

Fig. 9 - Microstructures of the transition zone in the AS and the RS for AA2024 and AA7075 T- joint welded at 800 rpm and 75 mm/min

3.2 Mechanical Properties

For as received alloys, the hardening mechanism in 2024-T4 ascribes to the present of Guinier-Preston zones (GP zones) that prevent dislocation movement. Al_2CuMg (spheroidized), Al_7Cu_2Fe (irregular), and Al_2Cu precipitates are the present phases in 2024-T4. This alloy has an average hardness equal to 135±5 *HV*. For 7075-T6 aluminum alloy the present phases are in irregular shapes of Al_7Cu_2Fe and Al_2CuMg. Moreover, spheroidal particles of Mg_2Si, and $MgZn_2$ precipitates at grain boundaries and inside the grain are presented. These precipitates produce an alloy 7075-T6 with average hardness equal to 165±5 *HV [11, 25, 30]*. The results of the hardness tests were highly dependent on the amount of mixing that occurred between the stringer (AA7075) and the skin (AA2024) materials during the welding

process. Hardness for all the tested conditions gave a (W) shape profile as shown in Fig. 12. The hardness profile emphasizes the change in microstructure and mechanical properties between the FSW zones. The higher values in the middle of the graph represent the SZ while the lower values represent the HAZ. Overall, these findings are in accordance with findings reported by Raja et al.[31]. However, when comparing our results to those of older studies, it must be pointed out that different conditions and alloys may show different hardness profiles when joint by FSW [32]. In Fig. 12, we also notice the variation in hardness between the upper surface of 2024AA (Row 1) which is directly under the tool shoulder, and the lower surfaces (Rows 2 and 3). The mixing in the first row was in 2024AA only. From that, we may conclude that the skin of the T-joint subjects to friction stir processing (FSP) [33]. Therefore, the closer the surface to the shoulder, the higher hardness is expected when comparing with other rows.

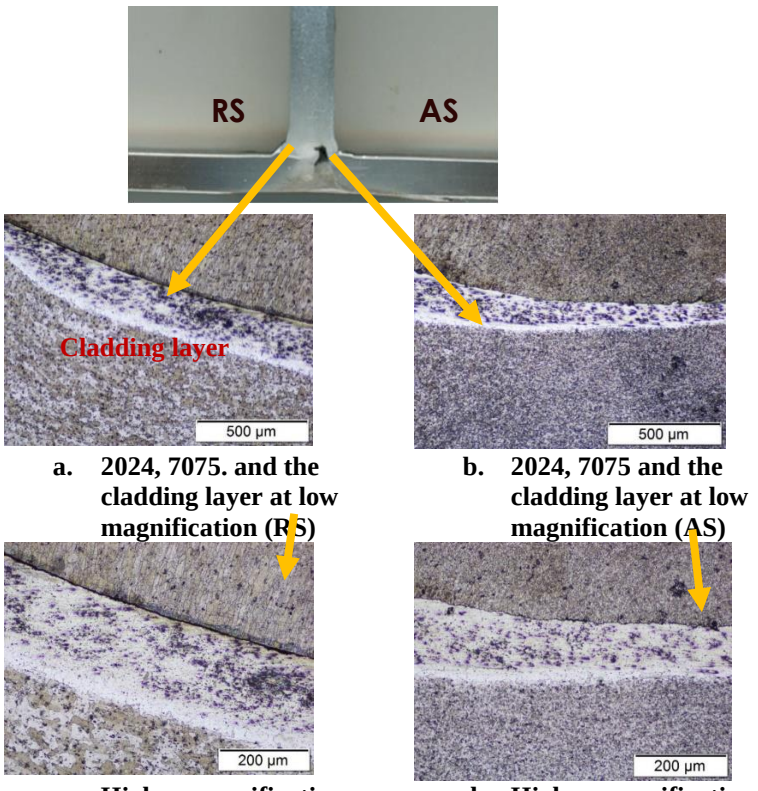

a. **2024, 7075. and the cladding layer at low magnification (RS)**

b. **2024, 7075 and the cladding layer at low magnification (AS)**

c. **Higher magnification (RS)**

d. **Higher magnification (AS)**

Fig. 10 - Cladding layer for the RS and the AS for T-joint welded at 800 rpm with 50 mm/min

The value of hardness in the SZ affected by the used rotational and traversal speeds for example at 1000 rpm and 100 mm/min the measured hardness values were slightly higher than the base alloy 2024AA in row 1, as shown in Fig. 12. However, lower rotational rate and traversal speed gave hardness values less than the 2024AA as shown in

. The findings are directly in line with previous findings by Saeid et. al. [34]. The reasons why Stir zone has the highest hardness are as follows:

Table 4 - Average hardness values of the SZ for the different conditions at row one

Firstly, high temperature in this region causes an increase in the solid solubility of the alloying elements, due to the dissolution of the precipitate which leads to high lattice distortion. This lattice distortion increases the resistance to dislocation motion. Also, the high temperature forces the large precipitates to dissolve and then reprecipitate by natural aging after FSW [35]. Secondly, the phase transformation driving force and nucleation rate increase which encourages the formation of fine recrystallized grains. In addition, the diffusion rate of the solute elements increases, which leads to a uniform distribution of the solute elements [25]. However, some particles could cause reduce in hardness and strength due to the formation of coarse particles, such as Mg2Si. The Mg2Si particles hinder the alloying element dissolution in the matrix. Also, grain growth could happen which lead to deterioration in mechanical properties as noticed in the HAZ region [30].

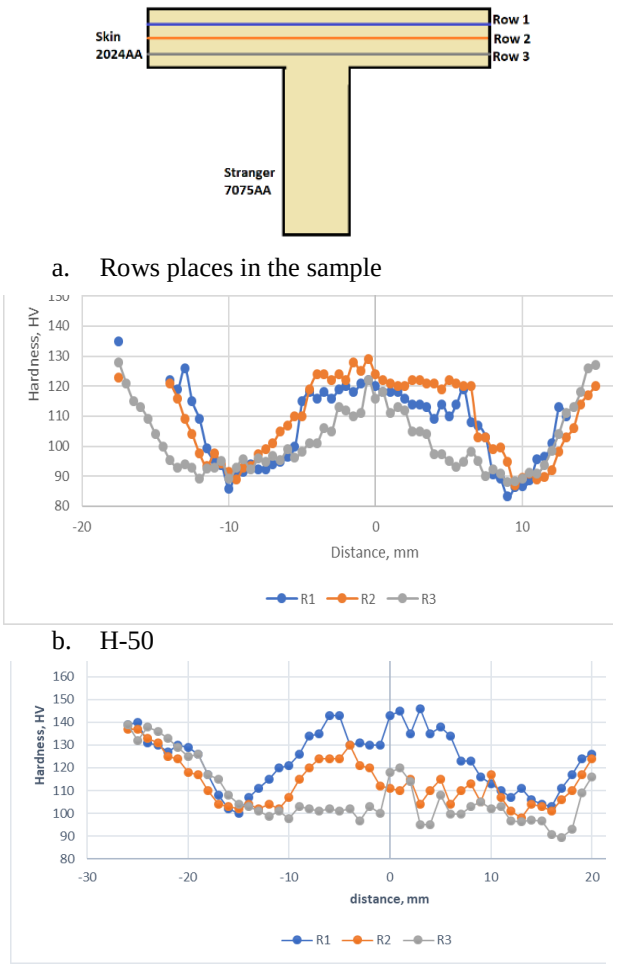

a. Rows places in the sample

b. H-50

c. H-100

Fig. 12 - Hardness measurements of the T-joint at different depths as shown in (a) for (b) H-50 (c) H-100

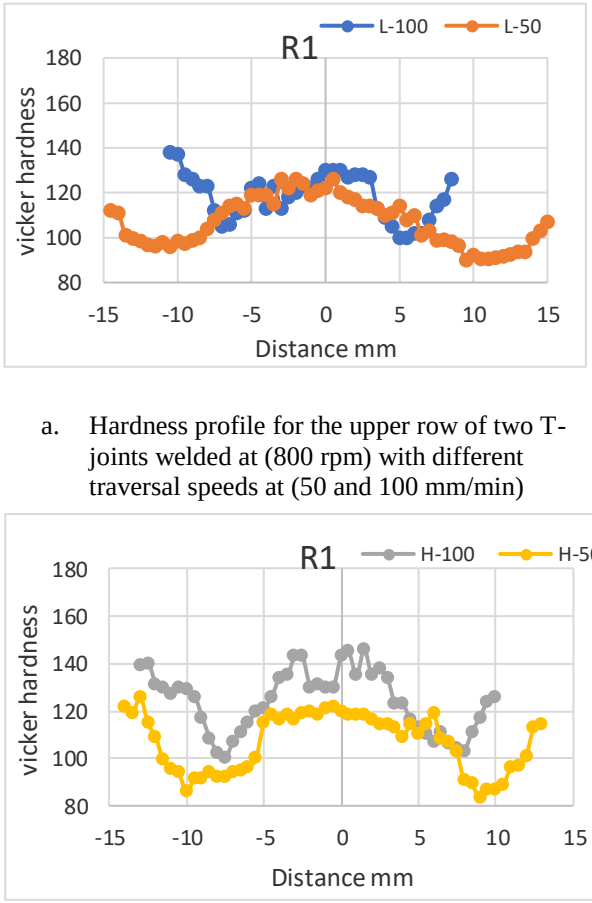

a. Hardness profile for the upper row of two T-joints welded at (800 rpm) with different traversal speeds at (50 and 100 mm/min)

b. Hardness profile for the first rows of two T-joint welded at (1000 rpm) with different traversal speeds at (50 and 100 mm/min)

Fig. 11 - Hardness profile comparison at constant rotational speed

Furthermore, low temperature in HAZ region during FSW compared to the solution temperature of the precipitates may lead to insufficient driving force for larger precipitates to dissolve, also in consequence to reprecipitate after FSW. Instead, some precipitates might have coarsened and lost their coherency with the matrix due to the thermal history which causes softening in the HAZ regions [2]. From Fig. 11, our results demonstrated that, at constant rotational rate, lower traversal speed increases the HAZ region and decreases the hardness values in this region[36]. low traversal speed gives wider hardness profile. This wider hardness profile means, wider HAZ region and wider SZ region which implies that lower traversal speed affects more surface area in FSW process. A similar pattern of wider HAZ region due to higher heat input was obtained in another research by AHMED et. al.[37]. This behavior has been attributed to the lower heat input at higher welding speed [35]. In contrary, at the same traversal speed and different rotational rates approximately the same hardness profile was shown as in Fig. **13**. However, the hardness values of the HAZ region are lower at higher rotational rate in both Fig. **13** (a) and (b).

From Fig. **14**, the hardness profile of the central line of the T-joint is illustrated. It is noticed a double trough in the curve with a maximum point between them which indicate the highest hardness value between the two curves, and it is approximately 145 HV. This abrupt increase of hardness is caused by the change of materials from AA2024-T4 to cladding layer then AA7075-T6. Also, from this figure, we noticed a HAZ region in 7075 aluminum alloy where the hardness values were declined until it reached approximately 115 *HV*, where the hardness value of 7075 was in the range of 165 *HV*.

The maximum failure load in X direction has the higher value when welded at high rotational rate of 1000 *rpm*, and low traversal speed 50 *mm/min*. However, this value is much lower than the base material for both AA 2024 and

AA 7075. The lower failure load value was obtained also at 1000 *rpm* but at higher traversal speed, 100 *mm/min* as shown in

.

Table 5 - Tensile test result along X and Y direction

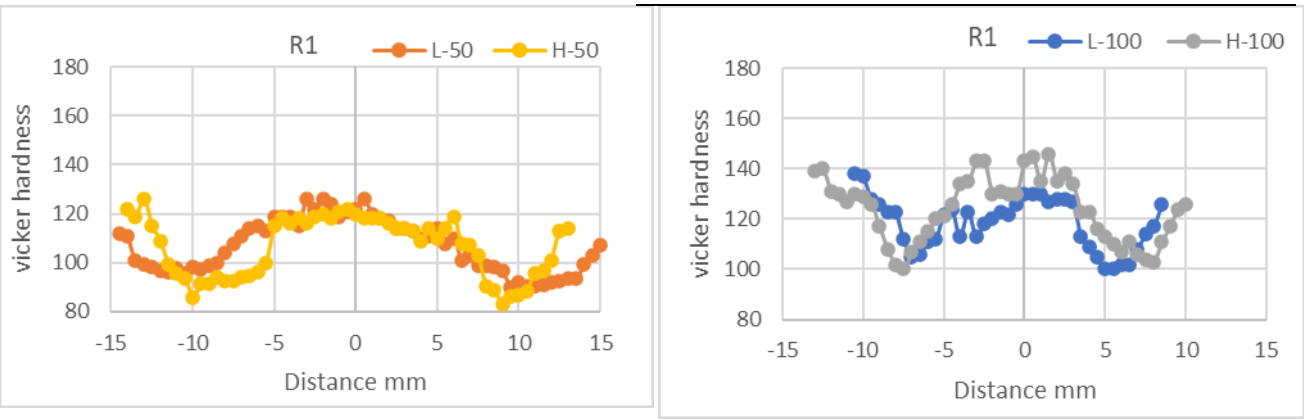

a. Hardness profile for the upper row of two T-joint welded (50 mm/min) but different rotational rate (800 and 1000 rpm)

b. Hardness profile for the upper row of two T-joint welded at (100 mm/min) but different rotational rate (800 and 1000 rpm)

Fig. 13 - Hardness profile comparison at constant traversal speed

Table 4 - Average hardness values of the SZ for the different conditions at row one

Sample ID	L-50	L-100	H-50	H-100
HV	122 ±3	124 ±6	118± 2	137 ± 6

Table 5 - Tensile test result along X and Y direction

Sample ID	Ultimate Tensile Strength (*MPa*)-X	Ultimate Tensile Strength (*MPa*)-Y
L-100	216.56	30.72
H-50	231.61	31.76
H-100	189.59	34.16

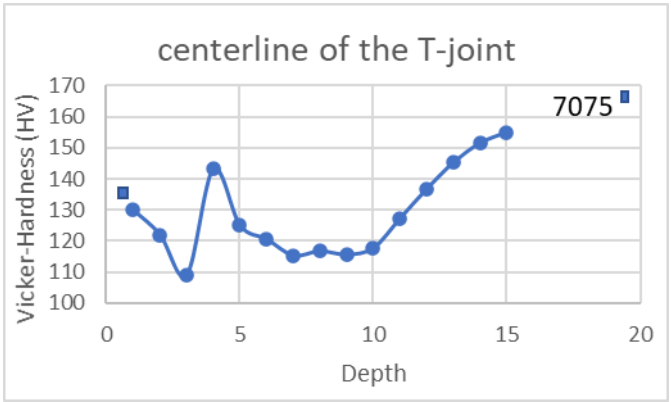

Fig. 14 - Hardness variation along the depth of the weldment of the T- joint at condition H-100

Conclusions

i. High quality defect free T-joints produced by using the higher (shoulder/pin ratio) D/d ratio of 4.31, at rotational rates of 800 and 1000 *rpm* and travel speeds of 50, 75 and 100 *mm/min.* Therefore, tool characterized by large shoulder diameter is preferred for this kind of joints.
ii. Significant grain refining was observed with the finest grain values of (4.6±0.8 μm) and (4.7±0.7 μm) resulted at constant rotational rate of 800 *rpm* with travel speeds of 50 and 100 *mm/min*, respectively. This result implies that rotational rate has more influence in grain size than the change in the travel speed.
iii. Wider W-shape hardness profile was shown at lower travel speed for given rotational rate.
iv. FSW process, shows asymmetric temperature distribution between the, AS and RS.
v. The highest hardness value of 137±6 *HV* at the SZ obtained at rotational rate of 1000 *rpm* and 100 mm/min at the SZ shows a high value up to 137±6 *HV* at rotational rate of 1000 *rpm* and 100 *mm/min.*
vi. The highest failure strength of 231.61 MPa value in the direction parallel to the skin (X direction) resulted at rotational rate of 1000 rpm and travel speed of 50 *mm/min.*
vii. The highest failure strength of 34.16 *MPa* value in the direction parallel to the stranger (Y-direction) resulted at rotational rate of 1000 *rpm* and travel speed of 100 *mm/min*.

Acknowledgements:

The authors would like to thank deeply Eng. Hager Amen for her support and help. Also, many thanks to the team in the Metallurgical and Materials Research Center of Scientific Excellence in Suez University,

References

[1] R. S. Mishra, P. S. De, and N. Kumar, "Friction Stir Processing," in *Friction Stir Welding and Processing: Science and Engineering*. Cham: Springer International Publishing, 2014, pp. 259-296.
[2] S. Verma, M. Gupta, and J. Misra, "Friction stir welding of aerospace materials: a state of art review," *Chapter*, vol. 13, pp. 135-150, 2016.
[3] B. T. Gibson *et al.*, "Friction stir welding: process, automation, and control," *Journal of Manufacturing Processes*, vol. 16, no. 1, pp. 56-73, 2014.
[4] P. Cavaliere, R. Nobile, F. Panella, and A. Squillace, "Mechanical and microstructural behaviour of 2024–7075 aluminium alloy sheets joined by friction stir welding," *International Journal of Machine Tools and Manufacture*, vol. 46, no. 6, pp. 588-594, 2006.
[5] M. M. Ahmed, S. Ataya, M. M. El-Sayed Seleman, A. Mahdy, N. A. Alsaleh, and E. Ahmed, "Heat Input and Mechanical Properties Investigation of Friction Stir Welded AA5083/AA5754 and AA5083/AA7020," *Metals*, vol. 11, no. 1, p. 68, 2021.
[6] R. S. Mishra and Z. Ma, "Friction stir welding and processing," *Materials science and engineering: R: reports*, vol. 50, no. 1-2, pp. 1-78, 2005.
[7] G. Padhy, C. Wu, and S. Gao, "Friction stir based welding and processing technologies-processes, parameters, microstructures and applications: A review," *Journal of Materials Science & Technology*, vol. 34, no. 1, pp. 1-38, 2018.
[8] M. Habba, M. Ahmed, M. M. Seleman, and A. EL-Nikhaily, "An Analytical Model of Heat Generation for Friction Stir Welding Using Bobbin Tool Design," *Journal of Petroleum and Mining Engineering*, vol. 20, no. 1, pp. 1-5, 2018.
[9] M. Ahmed, S. Ataya, M. Seleman, T. Allam, N. Alsaleh, and E. Ahmed, "Grain Structure, Crystallographic Texture, and Hardening Behavior of Dissimilar Friction Stir Welded AA5083-O and AA5754-H14. Metals 2021, 11, 181," ed: s Note: MDPI stays neutral with regard to jurisdictional claims in published …, 2021.
[10] G. Jadhav and R. Dalu, "Friction Stir Welding–Process Parameters and its Variables: A Review," *International Journal Of Engineering And Computer Science*, vol. 3, no. 06, 2014.
[11] G. Mrówka-Nowotnik and J. Sieniawski, "Analysis of intermetallic phases in 2024 aluminium alloy," in *Solid State Phenomena*, 2013, vol. 197: Trans Tech Publ, pp. 238-243.
[12] I. El-Mahallawi, M. Ahmed, A. Mahdy, A. Abdelmotagaly, W. Hoziefa, and M. Refat, "Effect of Heat treatment on friction-stir-processed nanodispersed AA7075 and 2024 Al Alloys," in *Friction Stir Welding and Processing IX*: Springer, 2017, pp. 297-309.
[13] W. Hoziefa *et al.*, "Influence of friction stir processing on the microstructure and mechanical properties of a compocast AA2024-Al2O3 nanocomposite," *Materials & Design*, vol. 106, pp. 273-284, 2016.
[14] L. Cui, X. Yang, G. Zhou, X. Xu, and Z. Shen, "Characteristics of defects and tensile behaviors on friction stir welded AA6061-T4 T-joints," *Materials Science and Engineering: A*, vol. 543, pp. 58-68, 2012.
[15] L. Dubourg, A. Merati, and M. Jahazi, "Process optimisation and mechanical properties of friction stir lap welds of 7075-T6 stringers on 2024-T3 skin," *Materials & Design*, vol. 31, no. 7, pp. 3324-3330, 2010.

[16] A. Pa, M. Ma, A. Na, D. R. Ka, and N. Sa, "Friction stir welded butt joints of AA2024 T3 and AA7075 T6 aluminum alloys," *Procedia Engineering*, vol. 75, pp. 98-102, 2014.
[17] M. Ahmed, M. El-Sayed Seleman, Z. Zidan, R. Ramadan, S. Ataya, and N. Alsaleh, "Microstructure and Mechanical Properties of Dissimilar Friction Stir Welded AA2024-T4/AA7075-T6 T-Butt Joints. Metals 2021, 11, 128," ed: s Note: MDPI stays neu-tral with regard to jurisdictional claims in …, 2021.
[18] F. Acerra, G. Buffa, L. Fratini, and G. Troiano, "On the FSW of AA2024-T4 and AA7075-T6 T-joints: an industrial case study," *The International Journal of Advanced Manufacturing Technology*, vol. 48, no. 9-12, pp. 1149-1157, 2010.
[19] M. Ahmed, S. Ataya, M. E.-S. Seleman, H. Ammar, and E. Ahmed, "Friction stir welding of similar and dissimilar AA7075 and AA5083," *Journal of Materials Processing Technology*, vol. 242, pp. 77-91, 2017.
[20] E. Raouache, Z. Driss, M. Guidara, and F. Khalfallah, "Effect of the Tool Geometries on Thermal Analysis of the Friction Stir Welding," *International Journal of Mechanics and Applications*, vol. 6, no. 1, pp. 1-7, 2016.
[21] N. Soni, S. Chandrashekhar, A. Kumar, and V. Chary, "Defects Formation during Friction Stir Welding: A Review," *International Journal of Engineering and Management Research (IJEMR)*, vol. 7, no. 3, pp. 121-125, 2017.
[22] P. Podržaj, B. Jerman, and D. Klobčar, "Welding defects at friction stir welding," *Metalurgija*, vol. 54, no. 2, pp. 387-389, 2015.
[23] A. Sedmak *et al.*, "Heat input effect of friction stir welding on aluminium alloy AA 6061-T6 welded joint," *Thermal Science*, vol. 20, no. 2, pp. 637-641, 2016.
[24] K. Jata and S. Semiatin, "Continuous dynamic recrystallization during friction stir welding of high strength aluminum alloys," Air force research lab wright-patterson afb oh materials and manufacturing …, 2000.
[25] C. Olea, L. Roldo, T. Strohaecker, and J. Dos Santos, "Friction stir welding of precipitate hardenable aluminium alloys: a review," *Welding in the World*, vol. 50, no. 11-12, pp. 78-87, 2006.
[26] J. Hou, H. Liu, and Y. Zhao, "Influences of rotation speed on microstructures and mechanical properties of 6061-T6 aluminum alloy joints fabricated by self-reacting friction stir welding tool," *The International Journal of Advanced Manufacturing Technology*, vol. 73, no. 5-8, pp. 1073-1079, 2014.
[27] J. Tang and Y. Shen, "Numerical simulation and experimental investigation of friction stir lap welding between aluminum alloys AA2024 and AA7075," *Journal of Alloys and Compounds*, vol. 666, pp. 493-500, 2016.
[28] K. Dudzik, "Properties of advancing side of weld in joint welded by FSW," *Journal of KONES*, vol. 21, no. 3, pp. 75--80, 2014.
[29] A. R. Raja, M. K. Yusufzai, and M. Vashista, "Characterization of advancing and retreating weld of friction stir welding of aluminium," ed: ICAMM, 2016.
[30] X.-l. Zou, Y. Hong, and X.-h. Chen, "Evolution of second phases and mechanical properties of 7075 Al alloy processed by solution heat treatment," *Transactions of Nonferrous Metals Society of China*, vol. 27, no. 10, pp. 2146-2155, 2017.
[31] S. Raja, F. Hasan, and A. H. Ansari, "Effect of Friction Stir Welding on the Hardness of Al-6061 T6 aluminium alloy," in *International Conference on Advanced Production and Industrial Engineering*, 2016, vol. 9, p. 10.
[32] J.-H. Kim, D.-S. Jo, and B.-M. Kim, "Hardness prediction of weldment in friction stir welding of AA6061 based on numerical approach," *Procedia engineering*, vol. 207, pp. 586-590, 2017.
[33] E. ELSayed, A. Mohamed, M. Ahmed, and A. EL-Nikhaily, "Effect of friction stir processing on the mechanical properties and microstructure of cast aluminum (Al-Si-Zn-Cu) Alloy," *Engineering research journal*, vol. 137, pp. 79-93, 2013.
[34] T. Saeid, A. Abdollah-Zadeh, H. Assadi, and F. M. Ghaini, "Effect of friction stir welding speed on the microstructure and mechanical properties of a duplex stainless steel," *Materials Science and Engineering: A*, vol. 496, no. 1-2, pp. 262-268, 2008.
[35] S. A. Khodir and T. Shibayanagi, "Microstructure and mechanical properties of friction stir welded dissimilar aluminum joints of AA2024-T3 and AA7075-T6," *Materials transactions*, pp. 0706110011-0706110011, 2007.
[36] T. S. Saad Ahmed Khodir, "Friction stir welding of dissimilar AA2024 and AA7075 aluminum alloys," vol. Materials Science and Engineering B, 2007.
[37] M. Ahmed, B. Wynne, W. Rainforth, A. Addison, J. Martin, and P. Threadgill, "Effect of tool geometry and heat input on the hardness, grain structure, and crystallographic texture of thick-section friction stir-welded aluminium," *Metallurgical and Materials Transactions A*, vol. 50, no. 1, pp. 271-284, 2019.